Polo-like kinase-1 regulates kinetochore–microtubule dynamics and spindle checkpoint silencing

Dan Liu, Olga Davydenko, and Michael A. Lampson

Department of Biology, University of Pennsylvania, Philadelphia, PA 19104

Polo-like kinase-1 (Plk1) is a highly conserved kinase with multiple mitotic functions. Plk1 localizes to prometaphase kinetochores and is reduced at metaphase kinetochores, similar to many checkpoint signaling proteins, but Plk1 is not required for spindle checkpoint function. Plk1 is also implicated in stabilizing kinetochore–microtubule attachments, but these attachments are most stable when kinetochore Plk1 levels are low at metaphase. Therefore, it is unclear how Plk1 function at kinetochores can be understood in the context of its dynamic localization. In this paper, we show that Plk1 activity suppresses kinetochore–microtubule dynamics to stabilize initial attachments in prometaphase, and Plk1 removal from kinetochores is necessary to maintain dynamic microtubules in metaphase. Constitutively targeting Plk1 to kinetochores maintained high activity at metaphase, leading to reduced interkinetochore tension and intrakinetochore stretch, a checkpoint-dependent mitotic arrest, and accumulation of microtubule attachment errors. Together, our data show that Plk1 dynamics at kinetochores control two critical mitotic processes: initially establishing correct kinetochore–microtubule attachments and subsequently silencing the spindle checkpoint.

Introduction

Polo-like kinase-1 (Plk1) regulates numerous processes in cell division and localizes to several intracellular sites based on interactions mediated by the Polo-box domain (PBD; Petronczki et al., 2008; Archambault and Glover, 2009). One of these sites is the kinetochore, where Plk1 is required for stable attachments to spindle microtubules (Sumara et al., 2004; Hanisch et al., 2006; Peters et al., 2006; Lénárt et al., 2007). However, Plk1 levels at kinetochores decrease dramatically when chromosomes align at metaphase (Lénárt et al., 2007), which is the time when kinetochore microtubules should be stabilized. The reduction of Plk1 levels at metaphase kinetochores is similar to the behavior of multiple mitotic checkpoint signaling proteins. Mad1 and Mps1, for example, are required for the spindle checkpoint, and their removal from kinetochores is important for checkpoint silencing (Jelluma et al., 2010; Maldonado and Kapoor, 2011). Plk1 is not a critical checkpoint signaling protein because its inhibition, either by RNAi or by a small molecule inhibitor, leads to a pronounced mitotic arrest as a result of checkpoint activation (Sumara et al., 2004; Lénárt et al., 2007). Because Plk1 reduction at kinetochores is puzzling in the context of regulating microtubule attachments and is apparently not an integral component of the spindle checkpoint, Plk1 function at kinetochores is unclear.

Results and discussion

To address the functional importance of dynamic Plk1 localization at kinetochores, we first tested whether the localization changes affect phosphorylation of a Plk1 substrate. We designed a fluorescence resonance energy transfer (FRET)–based phosphorylation sensor to track phosphorylation changes in live cells. A previously designed Plk1 phosphorylation sensor was specific for Plk1 in G2 but was phosphorylated by other kinases in mitosis (Fuller et al., 2008; Macůrek et al., 2008). Therefore, we tested several different substrate sequences from established Plk1 substrates (Johnson et al., 2007) in place of the Myt1 substrate previously used. Of multiple substrates tested, two were phosphorylated in mitosis in a Plk1-dependent manner (Figs. 1 A and S1 [A and B]), and we selected one of these from c-Jun for further experiments. To measure localized phosphorylation

Correspondence to Michael Lampson: lampson@sas.upenn.edu

Abbreviations used in this paper: FRET, fluorescence resonance energy transfer; PA, photoactivatable; PBD, Polo-box domain; wt, wild type.

The Rockefeller University Press $30.00
J. Cell Biol. Vol. 198 No. 4 491–499
www.jcb.org/cgi/doi/10.1083/jcb.201205090

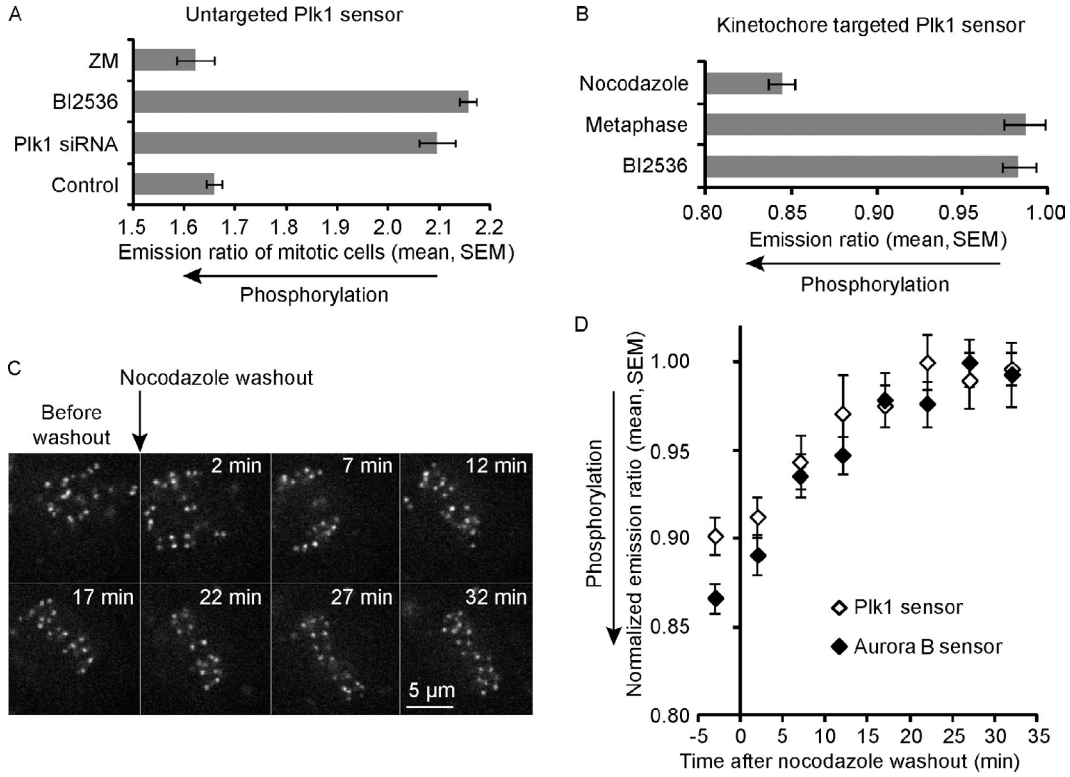

Figure 1. **A FRET-based biosensor for Plk1 activity at kinetochores is dephosphorylated as chromosomes align at metaphase.** (A) The YFP/CFP emission ratio was averaged over multiple mitotic cells ($n \geq 9$) expressing an untargeted Plk1 phosphorylation sensor and treated with an inhibitor for Aurora B (ZM) or Plk1 (BI2536) or with Plk1 siRNA, as indicated. (B) The YFP/TFP emission ratio was analyzed in cells expressing a kinetochore-targeted Plk1 sensor at metaphase or treated with nocodazole or BI2536, as indicated ($n \geq 10$ cells, $n \geq 15$ kinetochores per cell). (C and D) Cells expressing a kinetochore-targeted Plk1 sensor (C and D) or a kinetochore-targeted Aurora B sensor (D) were imaged live after nocodazole washout. Images (C) of the Plk1 sensor (YFP emission) show kinetochore alignment after washout. To compare FRET changes for the two sensors (D), the ratios for each were normalized by dividing by the maximum value for that sensor ($n \geq 10$ cells, $n \geq 15$ kinetochores per cell).

changes at kinetochores, we fused the sensor to the kinetochore protein Hec1. Cells were treated with nocodazole to depolymerize microtubules, which maintains high Plk1 levels on kinetochores, or analyzed at metaphase when kinetochore Plk1 levels are low. Phosphorylation of the kinetochore-targeted sensor was high in nocodazole and low in metaphase cells (Fig. 1 B), consistent with the differences in Plk1 localization. The dephosphorylation at metaphase likely reflects recruitment of protein phosphatase 1 (PP1; Liu et al., 2010) as well as reduced Plk1 levels.

We used the kinetochore-targeted Plk1 sensor to track phosphorylation dynamics as chromosomes align at metaphase, which is when kinetochore Plk1 levels decrease. For this assay, we arrested cells in mitosis with nocodazole and then removed the nocodazole to allow spindle formation. As kinetochores aligned at metaphase (Fig. 1 C), the Plk1 sensor was dephosphorylated (Fig. 1 D). For comparison, we also analyzed phosphorylation dynamics for a previously established kinetochore-targeted Aurora B sensor (Welburn et al., 2010), which was dephosphorylated with similar kinetics to the Plk1 sensor (Fig. 1 D). We also analyzed both Plk1 localization and phosphorylation of the Plk1 sensor after depletion of the kinetochore protein KNL1 by siRNA, which prevents PP1 recruitment to kinetochores at metaphase (Liu et al., 2010). Dephosphorylation of the Plk1 sensor depends on PP1 recruitment (Fig. S1 E), as previously shown for the Aurora B sensor (Liu et al., 2010), which indicates that substrates of both Plk1 and Aurora B are dephosphorylated in a PP1-dependent manner as chromosomes align at metaphase. In addition, removal of Plk1 from kinetochores at metaphase depends on PP1 recruitment (Fig. S1, C and D), consistent with a previous finding that loss of PP2A phosphatase increases Plk1 targeting to prometaphase kinetochores (Foley et al., 2011). In both cases, phosphatase levels are inversely correlated with Plk1 recruitment, consistent with a phosphorylation-dependent mechanism to regulate Plk1 localization, likely through PBD binding to phosphorylated kinetochore proteins (Elia et al., 2003).

To test the significance of Plk1 substrate dephosphorylation at kinetochores, we designed a strategy to constitutively target Plk1 to kinetochores by fusing the kinase to Hec1 (Fig. 2 A). We incorporated the activating Plk1-T210D mutation into this chimeric protein (Hec1-Plk1^{T210D}) to ensure that the kinase would be active (Lee and Erikson, 1997). In cells expressing Hec1-Plk1^{T210D}, KNL1 localized normally, indicating that the outer kinetochore is intact (Fig. S1 F). A kinetochore-targeted Plk1 sensor remained phosphorylated even on aligned chromosomes in these cells, indicating that maintaining Plk1 localization at kinetochores also maintains phosphorylation of Plk1 substrates (Fig. 2 B). In contrast, phosphorylation of a kinetochore-targeted Aurora B sensor

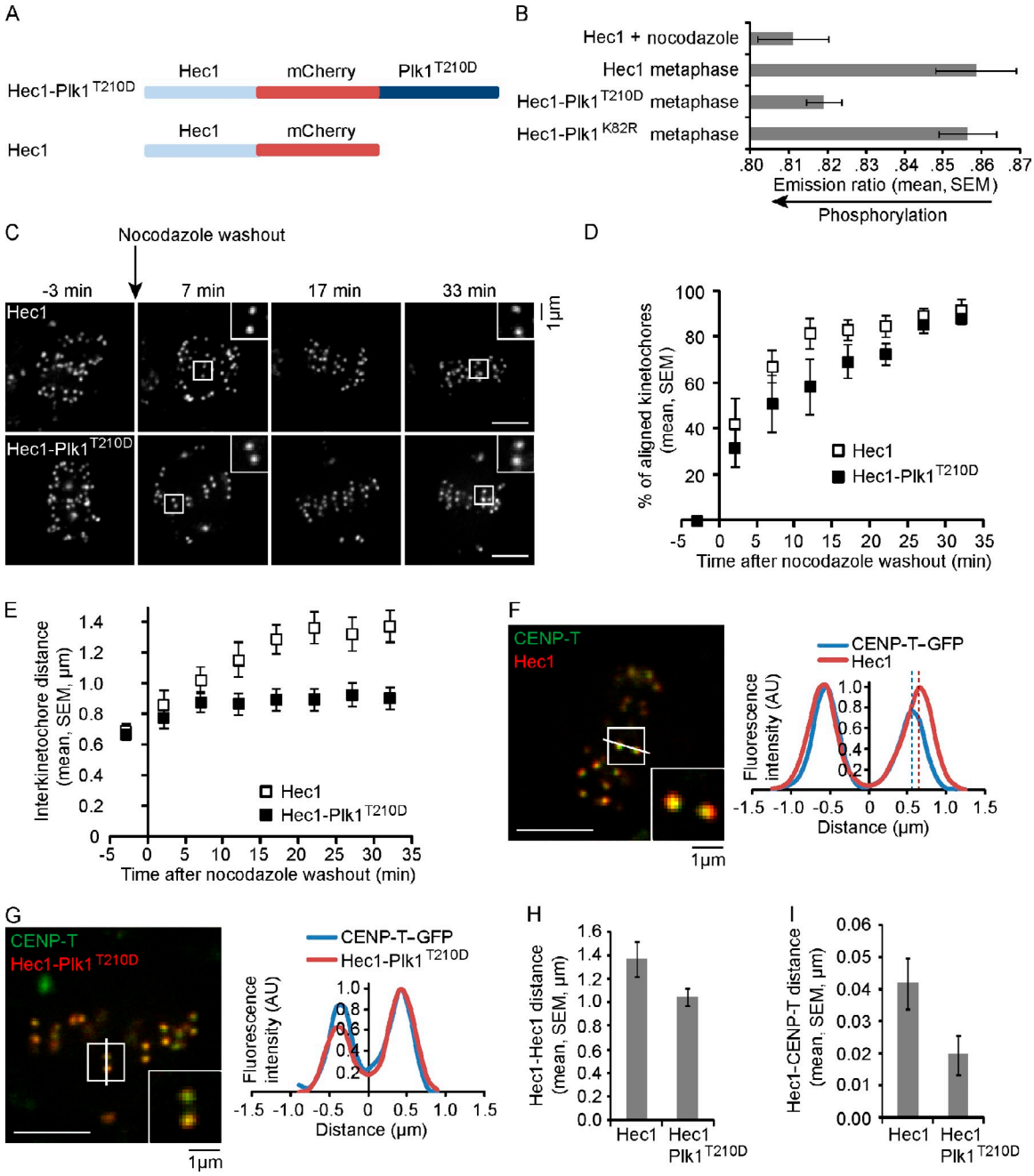

Figure 2. **Persistent Plk1 activity at kinetochores disrupts both interkinetochore tension and intrakinetochore stretch.** (A) Schematic of Hec1 and Hec1-Plk1^{T210D} constructs. (B) The YFP/TFP emission ratio was analyzed in cells expressing a kinetochore-targeted Plk1 phosphorylation sensor, together with either Hec1, Hec1-Plk1^{T210D}, or Hec1-Plk1^{K82R} (kinase-inactive mutant), under the conditions indicated ($n \geq 10$ cells, $n \geq 15$ kinetochores per cell). (C–E) Cells expressing either Hec1 or Hec1-Plk1^{T210D} were imaged live after nocodazole washout. Images (C) are maximal intensity projections of confocal z series. Insets are optical sections showing individual kinetochore pairs. Note that Hec1-Plk1^{T210D} localizes to both kinetochores and spindle poles. Metaphase alignment (D) and interkinetochore distance (E) were calculated at each time point ($n \geq 40$ kinetochores per time point from multiple cells). (F–I) Cells expressing CENP-T–GFP, together with either Hec1 or Hec1-Plk1^{T210D}, were imaged live at metaphase. Images (F and G) are single confocal planes, and insets show individual kinetochore pairs used for the line scans. Dashed lines indicate estimated Hec1 and CENP-T positions. Distances were calculated between sister kinetochores (H) or between Hec1 and CENP-T within a kinetochore ($n \geq 80$ kinetochore pairs from multiple cells; I). AU, arbitrary unit. (C, F, and G) Bars, 5 µm.

was not affected by expression of Hec1-Plk1^{T210D} (Fig. S2 C). We also examined phosphorylation of a known Plk1 substrate at kinetochores, BubR1-S676 (Elowe et al., 2007), and found increased phosphorylation in cells expressing Hec1-Plk1^{T210D} (Fig. S2, A and B). Together, these results indicate that Hec1-Plk1^{T210D} targets kinetochore Plk1 substrates specifically.

To determine how increased Plk1 activity affects kinetochore function, we repeated the nocodazole washout assay with cells expressing Hec1-Plk1^{T210D} or wild type (wt)–Hec1 as a control. In both cases, kinetochores aligned at the metaphase plate within ~30 min of nocodazole washout, although alignment is more efficient in cells expressing wt-Hec1 compared

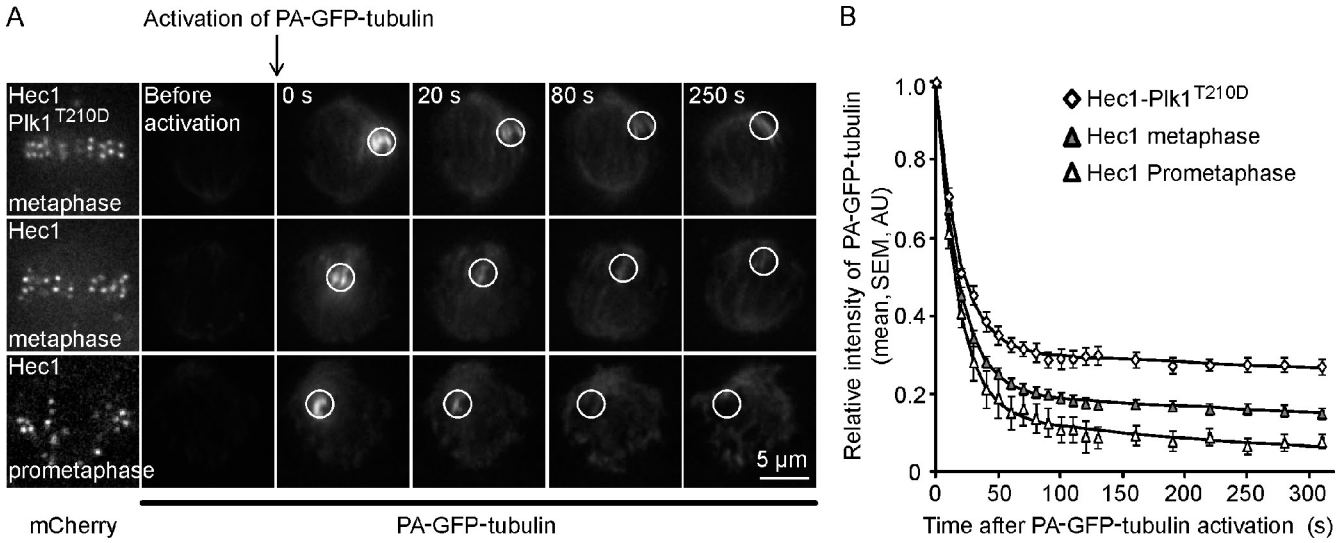

C

Double-exponential curve fitting: $\text{Intensity} = P_f \times e^{(-K_f \times t)} + P_s \times e^{(-K_s \times t)}$

	P_f (fast)	K_f (fast)	P_s (slow)	K_s (slow)	$t_{1/2f} = \ln 2/K_f$	$t_{1/2s} = \ln 2/K_s$
Hec1 metaphase	0.79	0.056	0.21	0.00105	12.5 s	661 s
Hec1 prometaphase	0.85	0.059	0.15	0.00284	11.8 s	244 s
Hec1-Plk1^{T210D}	0.69	0.055	0.31	0.00046	12.6 s	1506 s

Figure 3. **Persistent Plk1 activity at kinetochores suppresses microtubule dynamics.** (A) Cells expressing PA-GFP-tubulin together with either Hec1 or Hec1-Plk1^{T210D} were imaged live before and after photoactivation of a spot near the metaphase plate at t = 0. Images show PA-GFP-tubulin or Hec1 or Hec1-Plk1^{T210D} visualized with mCherry. (B) GFP intensity in the activated spot (white circles in A) was calculated at each time point as the intensity relative to the initial value after activation. The relative GFP intensities were corrected for photobleaching based on a taxol control, averaged over multiple cells ($n \geq 8$), and fit with double-exponential decay curves. AU, arbitrary unit. (C) Curve-fitting parameters K_f and K_s represent the fast and slow time constants, respectively.

with Hec1-Plk1^{T210D} (Fig. 2, C and D). Cells expressing wt-Hec1 established interkinetochore tension, measured as the distance between sister kinetochores (1.4 ± 0.1 µm), as the kinetochores aligned. In contrast, cells expressing Hec1-Plk1^{T210D} failed to establish tension (mean interkinetochore distance 0.9 ± 0.1 µm; Fig. 2 E), even though kinetochores were aligned at the metaphase plate. These results indicate that spindle microtubules fail to exert normal pulling forces on sister kinetochores when Plk1 activity remains high at metaphase kinetochores.

In addition to interkinetochore tension, deformations also occur within kinetochores and have been implicated in spindle checkpoint silencing (Maresca and Salmon, 2009; Uchida et al., 2009). We examined these deformations, referred to as intrakinetochore stretch, using CENP-T tagged at its C terminus with GFP and Hec1 tagged at its C terminus with mCherry to label the inner and outer kinetochore, respectively (Fig. 2, F and G). The positions of CENP-T and Hec1 were determined from the peak fluorescence intensities along a line between two sister kinetochores, and the intrakinetochore stretch was calculated as the distance between Hec1 and CENP-T within a kinetochore. The intrakinetochore stretch was dramatically reduced in cells expressing Hec1-Plk1^{T210D} (0.020 ± 0.006 µm) compared with control cells expressing wt-Hec1 (0.042 ± 0.008 µm; Fig. 2 I). The interkinetochore tension, calculated as the distance between Hec1 spots of sister kinetochores (Fig. 2 H), was also decreased in cells expressing Hec1-Plk1^{T210D} as in the nocodazole washout experiment (Fig. 2 E). In contrast, expression of Hec1-Plk1^{K82R}, a kinase-inactive mutant, did not decrease either interkinetochore tension or intrakinetochore stretch (Fig. S2, D–G). Both interkinetochore tension and intrakinetochore stretch decrease in the presence of either taxol or a low dose of nocodazole (Maresca and Salmon, 2009; Uchida et al., 2009), suggesting that both depend on dynamic microtubules (Khodjakov and Pines, 2010). Therefore, our findings suggest that Plk1 activity at kinetochores regulates microtubule dynamics.

To directly test whether maintaining Plk1 activity at metaphase kinetochores affects microtubule dynamics, we measured microtubule turnover using photoactivatable (PA) GFP-tubulin (PA-GFP-tubulin). After activating a spot within the spindle close to the metaphase plate, we followed the decrease of fluorescence in that spot over time (Fig. 3, A and B). Cells treated with taxol were used as controls to correct for photobleaching, as microtubule turnover should be negligible in the presence of taxol. The decrease in fluorescence after photoactivation is well fit by a double-exponential curve, with a fast phase representing nonkinetochore microtubules and a slow phase representing the more stable kinetochore microtubules (Mitchison, 1989; Zhai et al., 1995). In cells expressing wt-Hec1, the half-life of kinetochore microtubules was increased in metaphase cells relative to prometaphase (661 vs. 244 s), as expected, and further increased

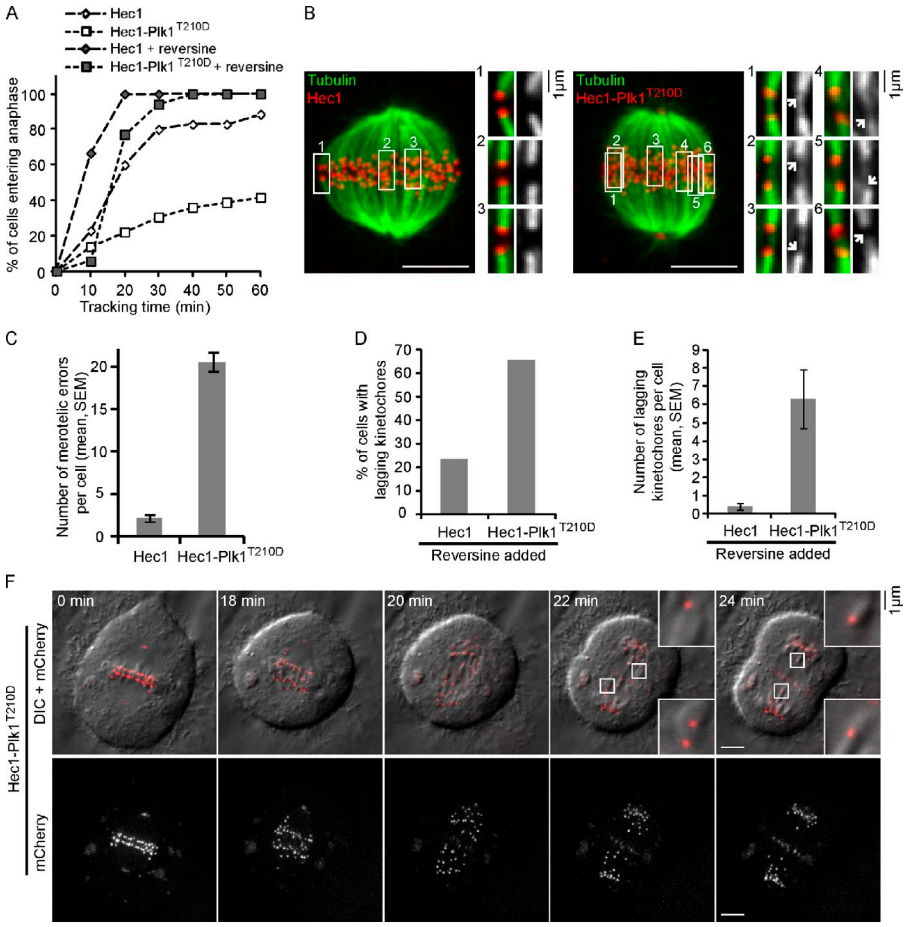

Figure 4. **Kinetochores with persistent Plk1 activity accumulate microtubule attachment errors and fail to silence the spindle checkpoint.** (A) Cells expressing either Hec1 or Hec1-Plk1^{T210D} were selected at metaphase and followed for 60 min to determine the time of anaphase onset (n > 20). The Mps1 inhibitor reversine was added, as indicated, at t = 0 to override the spindle checkpoint. (B and C) Cells expressing Hec1 or Hec1-Plk1^{T210D} were briefly permeabilized and treated with calcium to remove nonkinetochore microtubules, fixed, and stained for microtubules. Images (B) are maximal intensity projections of confocal z series. Insets show sister kinetochore pairs in optical sections. Images are scaled differently in the insets to show merotelic attachments (arrows) more clearly. The number of kinetochores with microtubules attached from both directions (merotelic errors) was determined (n = 20 cells; C). (D–F) For cells treated with reversine at metaphase, as in A, the fraction of cells with lagging kinetochores in anaphase (D) and the number of laggers per cell (E) were determined (n > 20). Images (F) show a representative cell expressing Hec1-Plk1^{T210D} with lagging kinetochores in anaphase. Insets show lagging kinetochores at higher magnification. Note that Hec1-Plk1^{T210D} localizes to kinetochores and spindle poles and to the anaphase spindle midzone. DIC, differential interference contrast. (B and F) Bars, 5 µm.

by over twofold in metaphase cells expressing Hec1-Plk1^{T210D} (1,506 s). The half-lives of nonkinetochore microtubules were similar in each case (Fig. 3 C). These results show that maintaining Plk1 activity at metaphase kinetochores suppresses microtubule dynamics, consistent with our findings of reduced interkinetochore tension and intrakinetochore stretch.

To test whether the suppression of microtubule dynamics and intrakinetochore stretch affects spindle checkpoint silencing, we measured the time spent in metaphase for cells expressing either wt-Hec1 or Hec1-Plk1^{T210D}. Cells with chromosomes aligned at the metaphase plate were selected and tracked for 60 min to determine the time of anaphase onset (Videos 1 and 2). Only 30% of cells expressing Hec1-Plk1^{T210D} entered anaphase within 30 min compared with 80% of cells expressing wt-Hec1 (Fig. 4 A). To test whether the metaphase arrest is a result of activation of the spindle checkpoint, we treated cells with reversine, a chemical inhibitor of the Mps1 kinase (Santaguida et al., 2010). Inhibition of Mps1 accelerated progress through metaphase of cells expressing wt-Hec1 (Fig. 4 A), consistent with the known requirement of Mps1 for checkpoint function. Strikingly, 94% of cells expressing Hec1-Plk1^{T210D} entered anaphase within 30 min after Mps1 inhibition, indicating that the spindle checkpoint was responsible for the metaphase arrest. Furthermore, Mad2-GFP is present on multiple metaphase kinetochores in cells expressing Hec1-Plk1^{T210D}, consistent with continued checkpoint activation (Fig. S2, H and I). Overall, the effects of increased Plk1 activity at kinetochores are similar in several respects to the effects of taxol: reduced microtubule dynamics, reduced interkinetochore tension and intrakinetochore stretch, and failure to silence the spindle checkpoint.

In addition to effects on the spindle checkpoint, microtubules must be dynamic to allow correction of kinetochore–microtubule attachment errors (Bakhoum et al., 2009a,b). To test whether high Plk1 activity at metaphase kinetochores promotes attachment errors, cells were fixed after brief treatment with calcium to destabilize nonkinetochore microtubules, leaving kinetochore microtubules intact. Cells expressing Hec1-Plk1^{T210D} contained large numbers of merotelic attachment errors (20.6 ± 1.1 per cell), in which a single kinetochore is attached to both spindle poles, whereas these errors were rare (2.3 ± 0.4 per cell) in cells expressing wt-Hec1 (Fig. 4, B and C). Merotelic errors are often associated with lagging chromosomes in anaphase because the kinetochore is pulled in both directions (Cimini et al., 2001). We examined anaphase segregation in cells that were treated with reversine at metaphase to bypass the checkpoint arrest. Cells expressing Hec1-Plk1^{T210D} frequently exhibited lagging chromosomes in anaphase (6.3 ± 1.6 per cell) compared with cells expressing wt-Hec1 (0.4 ± 0.2 per cell; Fig. 4 [D–F] and Videos 3–5). Merotelic microtubule attachments were also observed in fixed anaphase cells (Fig. S3 A). Together, these findings indicate that maintaining Plk1 activity at metaphase kinetochores disrupts two essential processes in metaphase: spindle checkpoint silencing and correction of merotelic attachment errors.

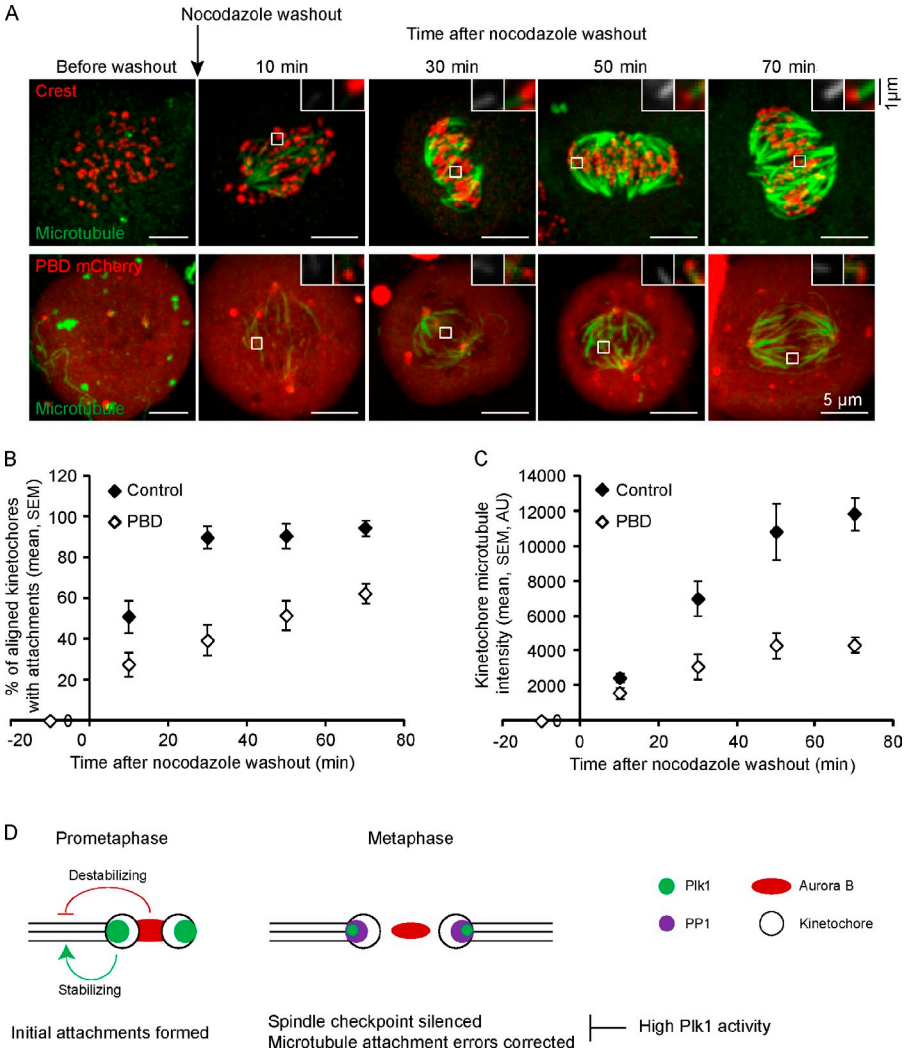

Figure 5. **Plk1 activity at kinetochores is required for efficient formation of stable kinetochore–microtubule attachments.** (A–C) Cells expressing PBD-mCherry or untransfected controls were fixed at the indicated time points after nocodazole washout and analyzed for cold-stable microtubules. Images (A) are maximal intensity projections of confocal z series. Insets are optical sections showing individual kinetochores. The PBD-mCherry images are scaled differently in the insets to show kinetochores more clearly. The fraction of aligned kinetochores with cold-stable attachments (B) and the microtubule staining intensities adjacent to kinetochores (C) were determined at each time point ($n \geq 10$ cells, $n \geq 30$ kinetochores per cell). AU, arbitrary unit. (D) A model showing that Aurora B and Plk1 activities are both high in prometaphase and have opposite effects on kinetochore microtubules, with Aurora B destabilizing and Plk1 stabilizing. In metaphase, both Aurora B and Plk1 activities are reduced at kinetochores, whereas PP1 is recruited. The reduction of Plk1 activity is important for maintaining dynamic microtubules, establishing intrakinetochore stretch and interkinetochore tension, silencing the spindle checkpoint, and correcting attachment errors (which can also occur in prometaphase).

Our findings address the question of why Plk1 is removed from metaphase kinetochores to maintain dynamic microtubules but raise the question of why Plk1 levels are high at prometaphase kinetochores. We considered the possibility that Plk1 activity stabilizes microtubules to promote formation of the initial attachments. To test this idea, we disrupted Plk1 targeting to kinetochores by overexpressing the PBD, which competes with endogenous Plk1 for kinetochore binding (Hanisch et al., 2006). GFP-Plk1 localizes to centrosomes in cells expressing moderate levels of PBD-mCherry but fails to localize to kinetochores (Fig. S3 B), indicating the Plk1 function is specifically disrupted at kinetochores. Furthermore, staining with a phosphospecific antibody showed that phosphorylation of BubR1-S676, a known Plk1 substrate at kinetochores (Elowe et al., 2007), was severely reduced in cells expressing PBD-mCherry, whereas total kinetochore BubR1 levels were unchanged (Fig. S3, C–F). We used the nocodazole washout assay to determine how efficiently kinetochores establish stable microtubule attachments during spindle formation. At time points up to 70 min after nocodazole washout, we measured the fraction of kinetochores aligned at the metaphase plate with cold-stable microtubule fibers and the microtubule staining intensity adjacent to these kinetochores (Fig. 5, A–C). Cells expressing the PBD established cold-stable attachments much more slowly than control cells (Fig. 5 B), with severely reduced tubulin staining at those kinetochores that do have attachments (Fig. 5 C). A previous result showed that cells expressing the PBD contain a few unattached kinetochores (Hanisch et al., 2006), but because PBD overexpression leads to a mitotic arrest, the cells have a long time to establish stable attachments. The nocodazole washout assay provides information about how attachments are stabilized over time, starting from the early stages of spindle assembly. Our results show that stabilization of the initial kinetochore–microtubule interactions in prometaphase depends on Plk1 activity at kinetochores.

Conclusions

Current models for regulation of kinetochore–microtubule interactions focus on tension-dependent changes in Aurora B kinase activity at kinetochores (Kelly and Funabiki, 2009; Santaguida and Musacchio, 2009; Lampson and Cheeseman, 2011). Aurora B has a well-established function in destabilizing attachments, and a large body of work has shown that multiple

Aurora B substrates at kinetochores participate in this process (Kelly and Funabiki, 2009; Lampson and Cheeseman, 2011). Because Aurora B substrates are highly phosphorylated in the low-tension state (DeLuca et al., 2006; Liu et al., 2009; Welburn et al., 2010; Salimian et al., 2011), it has been unclear how stable attachments initially form in prometaphase. Our findings provide a resolution to this question: Plk1 activity is high at prometaphase kinetochores and stabilizes kinetochore microtubules to balance the destabilizing activity of Aurora B. Another factor contributing to the initial stabilization is the recruitment of PP2A to prometaphase kinetochores, which can dephosphorylate Aurora B substrates (Foley et al., 2011). Many Plk1 substrates and interacting proteins have been identified at kinetochores (Petronczki et al., 2008; Archambault and Glover, 2009; Hegemann et al., 2011; Kettenbach et al., 2011; Hood et al., 2012), and unraveling their various contributions to regulating microtubule dynamics will be an important subject for future investigation.

Formation of stable attachments depends on Plk1 activity at kinetochores early in mitosis, but subsequent removal of this activity is critical for maintaining dynamic microtubules at bioriented kinetochores. Successful completion of mitosis depends on both correcting attachment errors and silencing the spindle checkpoint, and both processes fail if Plk1 activity remains high in metaphase. The increased microtubule stability and merotelic attachments (Figs. 3 and 4) are similar to defects observed in chromosomally unstable cancer cells (Bakhoum et al., 2009a,b) and suggest an explanation for the increased Plk1 expression in many cancers (Strebhardt and Ullrich, 2006). In addition, our findings provide insight into the regulation of intrakinetochore stretch, which is an important factor in spindle checkpoint silencing (Maresca and Salmon, 2009; Uchida et al., 2009), through Plk1-dependent changes in microtubule dynamics.

We show that phosphorylation of Plk1 and Aurora B biosensors change in parallel as chromosomes align (Fig. 1 D), consistent with previous findings that endogenous substrates are phosphorylated at prometaphase kinetochores and dephosphorylated at metaphase (DeLuca et al., 2006; Elowe et al., 2007; Welburn et al., 2010; Salimian et al., 2011). Proper regulation of kinetochore microtubules depends on a dynamic balance between the two kinases (Fig. 5 D), and both interact with INCENP (Goto et al., 2006; Carmena et al., 2012). Plk1 and Aurora B activities have opposite effects on kinetochore–microtubule dynamics, as either Aurora B inhibition (Cimini et al., 2006) or increased Plk1 activity (Fig. 3) suppresses microtubule turnover. Despite the apparent similarity, however, the effects of these perturbations are not the same. High Plk1 activity leads to reduced interkinetochore tension and intrakinetochore stretch (Fig. 2). In contrast, interkinetochore tension is not affected by partial Aurora B inhibition and is increased by mutation of Aurora B target sites in Hec1 (Cimini et al., 2006; DeLuca et al., 2006). These observations suggest that two different modes of regulating kinetochore microtubules depend on two highly conserved mitotic kinases. Aurora B function has been extensively studied, but major open questions remain regarding Plk1 substrates, their interactions with microtubules, and mechanisms controlling the dynamic Plk1 localization at kinetochores.

Materials and methods

Cell culture, transfection, and inhibitors

HeLa cells were cultured in growth medium: DME with 10% FBS and penicillin-streptomycin at 37°C in a humidified atmosphere with 5% CO_2. Cells were transfected with plasmid DNA using FuGENE (Roche) according to the manufacturer's instructions and then used for analysis 2 d after transfection. The Plk1 inhibitor BI2536 was used at 100 nM. Taxol was used at 10 µM. The Mps1 inhibitor reversine was used at 500 nM, which does not inhibit Aurora B in live cells (Santaguida et al., 2010). The siRNA oligonucleotides targeting Plk1 (5′-CGAGCUGCUUTTUGACGAGUU-3′; Kraft et al., 2003) and KNL1 (5′-GGAAUCCAAUGCUUUGAG-3′; Liu et al., 2010) were synthesized by Thermo Fisher Scientific.

Plasmids

The design of the Plk1 phosphorylation sensors is based on a protein kinase C sensor (Violin et al., 2003): a CFP/YFP FRET pair with a substrate peptide and an FHA2 phospho-Thr–binding domain in between. The Plk1 phosphorylation sensors were created by modifying previously reported untargeted and kinetochore-targeted Aurora B sensors (Fuller et al., 2008; Welburn et al., 2010). The amino acid sequence DDALNA*T*FLPSEG from c-Jun was used as a Plk1 substrate (Johnson et al., 2007), with Thr replacing Ser at position 17 (italicized) to match the requirement for FHA2 binding (Durocher et al., 2000), instead of the Aurora B substrate sequence in the previous sensors. The second sequence tested was PPSLSS*T*VLIVRN from BRCA2, with the Plk1 target Thr207 italicized and Thr203 mutated to Ser to prevent FHA2 binding to multiple sites. The kinetochore-targeted sensors, which contain mTFP1 (TFP) instead of CFP, as previously described (Liu et al., 2009), were fusions to either the N terminus of Hec1 or the C terminus of Mis12. The Hec1 fusion was used for all experiments, except that the Mis12 fusion was used in cells expressing Hec1-wt or Hec1-Plk1^{T210D} (Fig. 2 B). The untargeted and kinetochore-targeted (fusion to the N terminus of Hec1) Aurora B sensors follow the same basic design but with Aurora B substrate sequences, as previously described (Fuller et al., 2008; Welburn et al., 2010).

Hec1-mCherry was created by replacing GFP with mCherry in vector pEGFP-N1 and inserting Hec1 at the N terminus of mCherry. Hec1-mCherry-Plk1^{T210D} (referred to as Hec1-Plk1^{T210D}) was created by inserting the human Plk1 T210D mutant (a gift from B.H. Kwok, University of Montreal, Montreal, Quebec, Canada) at the C terminus of mCherry and Hec1 at the N terminus of mCherry in vector pCDNA3.1. GFP-Plk1 was a gift from B.H. Kwok. CENP-T–GFP was created by inserting CENP-T (a gift from I.M. Cheeseman, Whitehead Institute for Biomedical Research, Cambridge, MA) at the N terminus of GFP in the pEGFP-N1 vector. PBD-mCherry was created by inserting amino acids 326–603 of human Plk1 at the N terminus of mCherry in vector pEGFP-N1. PA-GFP-tubulin was a gift from J.M. Murray (University of Pennsylvania, Philadelphia, PA).

Live imaging and data analysis

For live imaging, cells were plated on 22 × 22–mm glass coverslips (no. 1.5; Thermo Fisher Scientific) coated with poly-D-lysine (Sigma-Aldrich). Coverslips were mounted in custom-designed Rose chambers using L-15 medium without phenol red (Invitrogen). Temperature was maintained at ∼35°C using either an air stream incubator (ASI 400; Nevtek) or an environmental chamber (Incubator BL; PeCon GmbH).

Live imaging of the kinetochore-targeted phosphorylation sensors was performed with a spinning-disk confocal microscope (DM4000; Leica) equipped with a 100× 1.4 NA objective, an XY Piezo-Z stage (Applied Scientific Instrumentation), a scanhead (CSU-10; Yokogawa Corporation of America), an electron multiplier charge-coupled device camera (ImageEM; Hamamatsu Photonics), and a laser merge module equipped with 440-, 488-, and 593-nm lasers (LMM5; Spectral Applied Research) controlled by MetaMorph software (Molecular Devices). TFP was excited at 440 nm, and TFP and YFP emissions were acquired simultaneously with a beam splitter (Dual-View; Optical Insights, LLC). Custom software written in MATLAB (MathWorks) was used for image analysis, as previously described (Fuller et al., 2008). In brief, individual kinetochores were defined automatically from confocal image stacks (five planes, 0.5-µm spacing), and the YFP/TFP emission ratio was calculated at each kinetochore. For single time point analyses, five z planes were acquired with 0.5-µm spacing. To measure dephosphorylation dynamics after nocodazole washout, a single image was taken at each time point to minimize photobleaching. The YFP/TFP emission ratios were calculated and averaged over multiple cells. Experiments were repeated multiple times ($n \geq 5$ for Figs. 1 B and 2 B, and $n = 2$ for Fig. 1 D) with similar results.

Live imaging of untargeted phosphorylation sensors was performed on a microscope (DM6000; Leica) with a 40× 1.25 NA objective and a charge-coupled device camera (ORCA-AG; Hamamatsu Photonics) controlled by MetaMorph software. CFP was excited with a CFP excitation filter, and CFP and YFP emissions were acquired sequentially by switching between CFP and YFP emission filters using a filter wheel (Ludl Electronic Products). The YFP/CFP emission ratio in each image was calculated after background subtraction and averaged over multiple cells. Experiments were repeated multiple times (n = 3 for Fig. 1 A, and n = 2 for Fig. S1 [A and B]) with similar results.

For nocodazole washout assays, cells were incubated in a low concentration of nocodazole (30 ng/ml) in growth medium for 0.5–1 h to disrupt the spindle. Cells were washed four times with fresh L-15 medium to remove nocodazole at time 0 to allow spindle formation. Using the spinning-disk confocal described in this section, one image was acquired every 5 min for the phosphorylation sensors or one image stack (three planes, 0.5-µm spacing) for Hec-mCherry or Hec1-mCherry-Plk1^{T210D}. Kinetochore alignment and interkinetochore distances (Fig. 2, D and E) were averaged over multiple cells from three independent experiments.

For interkinetochore distance and intrakinetochore stretch measurements (Fig. 2, F–I), images of CENP-T–GFP and Hec1-mCherry were acquired using the spinning-disk confocal described in this section. Fluorescence intensities of GFP and mCherry were measured along a line between the two sister kinetochores, and the position of peak intensity at each kinetochore was determined manually. The intrakinetochore stretch was calculated as the distance between the GFP peak and the mCherry peak within a single kinetochore. Results were averaged over multiple cells from four independent experiments.

To measure the time to anaphase and the frequency of lagging chromosomes (Fig. 4), cells were imaged every 2 min for 60 min (five z planes, 0.5-µm spacing at each time point) using the spinning-disk confocal described in this section. Lagging chromosomes were counted and averaged over multiple cells from three independent experiments.

Photoactivation assay

Photoactivation experiments were performed with the spinning-disk confocal described in the previous section, using a scanhead with a 405-nm laser (iLas; Roper Scientific). Cells transfected with PA-GFP-tubulin together with either Hec1-mCherry-Plk1 or Hec1-mCherry were imaged once before activation to determine the position of the kinetochores followed by activation of spindle microtubules adjacent to the metaphase plate. After activation, one image was acquired every 10 s initially and then every 30 s to minimize photobleaching. Only cells in which the activated spot stayed in focus for the duration of the experiment were further analyzed. Fluorescence intensities were measured at each time point in a circle defined by the size of the activated region using ImageJ software (National Institutes of Health). Background was subtracted by measuring the same pixel area adjacent to the spindle. The values were corrected for photobleaching by determining the fluorescence loss in activated cells treated with taxol (10 µM). Data were averaged over multiple cells and then fitted to a double-exponential curve, shown as $Y = P_f \exp(-K_f t) + P_s \exp(-K_s t)$, in which Y is the proportion of the initial fluorescence intensity, P is the proportion of fast (f) and slow (s) decay of fluorescence, K is the rate constant for fluorescence decay, and t is time. Curve fitting was performed using the curve fitting tool box in MATLAB. The turnover half-time ($t_{1/2}$) was calculated as ln2/k for each fast and slow process.

Cold-stable microtubule assay and immunofluorescence

To examine cold-stable microtubules, cells were incubated on ice for 10 min in L-15 medium with 20 mM Hepes, pH 7.3, fixed for 10 min at room temperature with 4% formaldehyde in 100 mM Pipes, pH 6.8, 10 mM EGTA, 1 mM $MgCl_2$, and 0.2% Triton X-100, and stained for tubulin using DM1-α antibody (1:3,000; Sigma-Aldrich) and CREST antiserum (1:10,000) with Alexa Fluor 488 and 594 secondary antibodies (1:1,000; Invitrogen). Images were acquired with the aforementioned spinning-disk confocal. To measure the intensities of microtubule plus ends at kinetochores, a line (width = 5 pixels) was drawn across the plus end of an individual kinetochore–microtubule fiber, close to the kinetochore. The maximal intensity across the line was determined using the Plot profile function of ImageJ, and intensities were averaged over multiple microtubule fibers after background subtraction.

To detect merotelic attachments, cells were permeabilized for 2 min at 37°C in 100 mM Pipes, pH 6.8, 1 mM $MgCl_2$, 0.1 mM $CaCl_2$, and 0.1% Triton X-100 and then fixed for 10 min in the same buffer supplemented with 4% formaldehyde. Cells were stained for tubulin using DM1-α antibody (1:3,000), and images were acquired with the aforementioned spinning-disk confocal. Merotelic errors were counted in multiple cells from three independent experiments.

To measure phosphorylation of BubR1, cells were incubated with nocodazole (100 ng/ml for 30 min), fixed with 4% formaldehyde in 100 mM Pipes, pH 6.8, 10 mM EGTA, 1 mM $MgCl_2$, and 0.2% Triton X-100, and stained with a phosphospecific antibody against BubR1 S676-P (1:1,000; a gift from S. Elowe, Centre de recherche du CHUQ, Québec, Canada) or an antibody against BubR1 (1:1,000; Abcam) together with CREST antiserum (1:10,000). Secondary antibodies were Alexa Fluor 488 and 593 (1:1,000; Invitrogen). KNL1 staining was performed with a rabbit pAb (a gift from I.M. Cheeseman).

Online supplemental material

Fig. S1 shows characterization of Plk1 phosphorylation sensors and Hec1-Plk1^{T210D}. Fig. S2 shows effects of Hec1-Plk1^{T210D} expression. Fig. S3 shows effects of Hec1-Plk1^{T210D} or PBD-mCherry expression. Video 1 shows a control cell expressing Hec1-mCherry, imaged from metaphase to anaphase. Video 2 shows a cell expressing Hec1-mCherry-Plk1^{T210D}, imaged from metaphase for 60 min with no anaphase onset. Video 3 shows a control cell expressing Hec1-mCherry, imaged from metaphase to anaphase with reversine added at t = 0. Video 4 shows a cell expressing Hec1-mCherry-Plk1^{T210D}, imaged from metaphase to anaphase with reversine added at t = 0, corresponding to the images shown in Fig. 4 F. Video 5 shows another example of a cell expressing Hec1-mCherry-Plk1^{T210D}, imaged from metaphase to anaphase with reversine added at t = 0. Online supplemental material is available at http://www.jcb.org/cgi/content/full/jcb.201205090/DC1.

We thank I.M. Cheeseman, B.H. Kwok, S. Elowe, and J.M. Murray for the kind gifts of reagents, B.E. Black for comments on the manuscript, and E. Ballister for experimental suggestions.

This work was supported by grants from the National Institutes of Health (GM083988) and the Searle Scholars Program to M.A. Lampson.

Author contributions: M.A. Lampson and D. Liu designed the experiments. D. Liu performed all experiments and data analysis except the construction and testing of untargeted Plk1 biosensors, which was performed by O. Davydenko. D. Liu and M.A. Lampson wrote the paper.

Submitted: 15 May 2012
Accepted: 17 July 2012

References

Archambault, V., and D.M. Glover. 2009. Polo-like kinases: Conservation and divergence in their functions and regulation. *Nat. Rev. Mol. Cell Biol.* 10:265–275. http://dx.doi.org/10.1038/nrm2653

Bakhoum, S.F., G. Genovese, and D.A. Compton. 2009a. Deviant kinetochore microtubule dynamics underlie chromosomal instability. *Curr. Biol.* 19: 1937–1942. http://dx.doi.org/10.1016/j.cub.2009.09.055

Bakhoum, S.F., S.L. Thompson, A.L. Manning, and D.A. Compton. 2009b. Genome stability is ensured by temporal control of kinetochore-microtubule dynamics. *Nat. Cell Biol.* 11:27–35. http://dx.doi.org/10.1038/ncb1809

Carmena, M., X. Pinson, M. Platani, Z. Salloum, Z. Xu, A. Clark, F. Macisaac, H. Ogawa, U. Eggert, D.M. Glover, et al. 2012. The chromosomal passenger complex activates Polo kinase at centromeres. *PLoS Biol.* 10:e1001250. http://dx.doi.org/10.1371/journal.pbio.1001250

Cimini, D., B. Howell, P. Maddox, A. Khodjakov, F. Degrassi, and E.D. Salmon. 2001. Merotelic kinetochore orientation is a major mechanism of aneuploidy in mitotic mammalian tissue cells. *J. Cell Biol.* 153:517–527. http://dx.doi.org/10.1083/jcb.153.3.517

Cimini, D., X. Wan, C.B. Hirel, and E.D. Salmon. 2006. Aurora kinase promotes turnover of kinetochore microtubules to reduce chromosome segregation errors. *Curr. Biol.* 16:1711–1718. http://dx.doi.org/10.1016/j.cub.2006.07.022

DeLuca, J.G., W.E. Gall, C. Ciferri, D. Cimini, A. Musacchio, and E.D. Salmon. 2006. Kinetochore microtubule dynamics and attachment stability are regulated by Hec1. *Cell*. 127:969–982. http://dx.doi.org/10.1016/j.cell.2006.09.047

Durocher, D., I.A. Taylor, D. Sarbassova, L.F. Haire, S.L. Westcott, S.P. Jackson, S.J. Smerdon, and M.B. Yaffe. 2000. The molecular basis of FHA domain:phosphopeptide binding specificity and implications for phospho-dependent signaling mechanisms. *Mol. Cell*. 6:1169–1182. http://dx.doi.org/10.1016/S1097-2765(00)00114-3

Elia, A.E., L.C. Cantley, and M.B. Yaffe. 2003. Proteomic screen finds pSer/pThr-binding domain localizing Plk1 to mitotic substrates. *Science*. 299:1228–1231. http://dx.doi.org/10.1126/science.1079079

Elowe, S., S. Hümmer, A. Uldschmid, X. Li, and E.A. Nigg. 2007. Tension-sensitive Plk1 phosphorylation on BubR1 regulates the stability of kinetochore microtubule interactions. *Genes Dev.* 21:2205–2219. http://dx.doi.org/10.1101/gad.436007

Foley, E.A., M. Maldonado, and T.M. Kapoor. 2011. Formation of stable attachments between kinetochores and microtubules depends on the B56-PP2A phosphatase. *Nat. Cell Biol.* 13:1265–1271. http://dx.doi.org/10.1038/ncb2327

Fuller, B.G., M.A. Lampson, E.A. Foley, S. Rosasco-Nitcher, K.V. Le, P. Tobelmann, D.L. Brautigan, P.T. Stukenberg, and T.M. Kapoor. 2008. Midzone activation of aurora B in anaphase produces an intracellular phosphorylation gradient. *Nature*. 453:1132–1136. http://dx.doi.org/10.1038/nature06923

Goto, H., T. Kiyono, Y. Tomono, A. Kawajiri, T. Urano, K. Furukawa, E.A. Nigg, and M. Inagaki. 2006. Complex formation of Plk1 and INCENP required for metaphase-anaphase transition. *Nat. Cell Biol.* 8:180–187. http://dx.doi.org/10.1038/ncb1350

Hanisch, A., A. Wehner, E.A. Nigg, and H.H. Silljé. 2006. Different Plk1 functions show distinct dependencies on Polo-Box domain-mediated targeting. *Mol. Biol. Cell*. 17:448–459. http://dx.doi.org/10.1091/mbc.E05-08-0801

Hegemann, B., J.R. Hutchins, O. Hudecz, M. Novatchkova, J. Rameseder, M.M. Sykora, S. Liu, M. Mazanek, P. Lénárt, J.K. Hériché, et al. 2011. Systematic phosphorylation analysis of human mitotic protein complexes. *Sci. Signal.* 4:rs12. http://dx.doi.org/10.1126/scisignal.2001993

Hood, E.A., A.N. Kettenbach, S.A. Gerber, and D.A. Compton. 2012. Plk1 regulates the kinesin-13 protein Kif2b to promote faithful chromosome segregation. *Mol. Biol. Cell*. 23:2264–2274. http://dx.doi.org/10.1091/mbc.E11-12-1013

Jelluma, N., T.B. Dansen, T. Sliedrecht, N.P. Kwiatkowski, and G.J. Kops. 2010. Release of Mps1 from kinetochores is crucial for timely anaphase onset. *J. Cell Biol.* 191:281–290. http://dx.doi.org/10.1083/jcb.201003038

Johnson, E.F., K.D. Stewart, K.W. Woods, V.L. Giranda, and Y. Luo. 2007. Pharmacological and functional comparison of the polo-like kinase family: Insight into inhibitor and substrate specificity. *Biochemistry*. 46:9551–9563. http://dx.doi.org/10.1021/bi7008745

Kelly, A.E., and H. Funabiki. 2009. Correcting aberrant kinetochore microtubule attachments: An Aurora B-centric view. *Curr. Opin. Cell Biol.* 21:51–58. http://dx.doi.org/10.1016/j.ceb.2009.01.004

Kettenbach, A.N., D.K. Schweppe, B.K. Faherty, D. Pechenick, A.A. Pletnev, and S.A. Gerber. 2011. Quantitative phosphoproteomics identifies substrates and functional modules of Aurora and Polo-like kinase activities in mitotic cells. *Sci. Signal.* 4:rs5. http://dx.doi.org/10.1126/scisignal.2001497

Khodjakov, A., and J. Pines. 2010. Centromere tension: A divisive issue. *Nat. Cell Biol.* 12:919–923. http://dx.doi.org/10.1038/ncb1010-919

Kraft, C., F. Herzog, C. Gieffers, K. Mechtler, A. Hagting, J. Pines, and J.M. Peters. 2003. Mitotic regulation of the human anaphase-promoting complex by phosphorylation. *EMBO J.* 22:6598–6609. http://dx.doi.org/10.1093/emboj/cdg627

Lampson, M.A., and I.M. Cheeseman. 2011. Sensing centromere tension: Aurora B and the regulation of kinetochore function. *Trends Cell Biol.* 21:133–140. http://dx.doi.org/10.1016/j.tcb.2010.10.007

Lee, K.S., and R.L. Erikson. 1997. Plk is a functional homolog of *Saccharomyces cerevisiae* Cdc5, and elevated Plk activity induces multiple septation structures. *Mol. Cell. Biol.* 17:3408–3417.

Lénárt, P., M. Petronczki, M. Steegmaier, B. Di Fiore, J.J. Lipp, M. Hoffmann, W.J. Rettig, N. Kraut, and J.M. Peters. 2007. The small-molecule inhibitor BI 2536 reveals novel insights into mitotic roles of polo-like kinase 1. *Curr. Biol.* 17:304–315. http://dx.doi.org/10.1016/j.cub.2006.12.046

Liu, D., G. Vader, M.J. Vromans, M.A. Lampson, and S.M. Lens. 2009. Sensing chromosome bi-orientation by spatial separation of aurora B kinase from kinetochore substrates. *Science*. 323:1350–1353. http://dx.doi.org/10.1126/science.1167000

Liu, D., M. Vleugel, C.B. Backer, T. Hori, T. Fukagawa, I.M. Cheeseman, and M.A. Lampson. 2010. Regulated targeting of protein phosphatase 1 to the outer kinetochore by KNL1 opposes Aurora B kinase. *J. Cell Biol.* 188:809–820. http://dx.doi.org/10.1083/jcb.201001006

Macůrek, L., A. Lindqvist, D. Lim, M.A. Lampson, R. Klompmaker, R. Freire, C. Clouin, S.S. Taylor, M.B. Yaffe, and R.H. Medema. 2008. Polo-like kinase-1 is activated by aurora A to promote checkpoint recovery. *Nature*. 455:119–123. http://dx.doi.org/10.1038/nature07185

Maldonado, M., and T.M. Kapoor. 2011. Constitutive Mad1 targeting to kinetochores uncouples checkpoint signalling from chromosome biorientation. *Nat. Cell Biol.* 13:475–482. http://dx.doi.org/10.1038/ncb2223

Maresca, T.J., and E.D. Salmon. 2009. Intrakinetochore stretch is associated with changes in kinetochore phosphorylation and spindle assembly checkpoint activity. *J. Cell Biol.* 184:373–381. http://dx.doi.org/10.1083/jcb.200808130

Mitchison, T.J. 1989. Polewards microtubule flux in the mitotic spindle: Evidence from photoactivation of fluorescence. *J. Cell Biol.* 109:637–652. http://dx.doi.org/10.1083/jcb.109.2.637

Peters, U., J. Cherian, J.H. Kim, B.H. Kwok, and T.M. Kapoor. 2006. Probing cell-division phenotype space and Polo-like kinase function using small molecules. *Nat. Chem. Biol.* 2:618–626. http://dx.doi.org/10.1038/nchembio826

Petronczki, M., P. Lénárt, and J.M. Peters. 2008. Polo on the rise-from mitotic entry to cytokinesis with Plk1. *Dev. Cell*. 14:646–659. http://dx.doi.org/10.1016/j.devcel.2008.04.014

Salimian, K.J., E.R. Ballister, E.M. Smoak, S. Wood, T. Panchenko, M.A. Lampson, and B.E. Black. 2011. Feedback control in sensing chromosome biorientation by the Aurora B kinase. *Curr. Biol.* 21:1158–1165. http://dx.doi.org/10.1016/j.cub.2011.06.015

Santaguida, S., and A. Musacchio. 2009. The life and miracles of kinetochores. *EMBO J.* 28:2511–2531. http://dx.doi.org/10.1038/emboj.2009.173

Santaguida, S., A. Tighe, A.M. D'Alise, S.S. Taylor, and A. Musacchio. 2010. Dissecting the role of MPS1 in chromosome biorientation and the spindle checkpoint through the small molecule inhibitor reversine. *J. Cell Biol.* 190:73–87. http://dx.doi.org/10.1083/jcb.201001036

Strebhardt, K., and A. Ullrich. 2006. Targeting polo-like kinase 1 for cancer therapy. *Nat. Rev. Cancer*. 6:321–330. http://dx.doi.org/10.1038/nrc1841

Sumara, I., J.F. Giménez-Abián, D. Gerlich, T. Hirota, C. Kraft, C. de la Torre, J. Ellenberg, and J.M. Peters. 2004. Roles of polo-like kinase 1 in the assembly of functional mitotic spindles. *Curr. Biol.* 14:1712–1722. http://dx.doi.org/10.1016/j.cub.2004.09.049

Uchida, K.S., K. Takagaki, K. Kumada, Y. Hirayama, T. Noda, and T. Hirota. 2009. Kinetochore stretching inactivates the spindle assembly checkpoint. *J. Cell Biol.* 184:383–390. http://dx.doi.org/10.1083/jcb.200811028

Violin, J.D., J. Zhang, R.Y. Tsien, and A.C. Newton. 2003. A genetically encoded fluorescent reporter reveals oscillatory phosphorylation by protein kinase C. *J. Cell Biol.* 161:899–909. http://dx.doi.org/10.1083/jcb.200302125

Welburn, J.P., M. Vleugel, D. Liu, J.R. Yates III, M.A. Lampson, T. Fukagawa, and I.M. Cheeseman. 2010. Aurora B phosphorylates spatially distinct targets to differentially regulate the kinetochore-microtubule interface. *Mol. Cell*. 38:383–392. http://dx.doi.org/10.1016/j.molcel.2010.02.034

Zhai, Y., P.J. Kronebusch, and G.G. Borisy. 1995. Kinetochore microtubule dynamics and the metaphase-anaphase transition. *J. Cell Biol.* 131:721–734. http://dx.doi.org/10.1083/jcb.131.3.721